ADVANCED MATERIALS INTERFACES
www.advmatinterfaces.de

Controllable Synthesis of Atomically Thin 1T-$SnSe_2$ Flakes and Its Linear Second Harmonic Generation with Layer Thickness

*Jiatian Fu, Liyun Zhao, Liang Zhou, Kang Wu, Jiaxing Du, Xiangzhuo Wang, Jiepeng Song, Lijie Zhu, Fan Zhou, Yahuan Huan, Lihong Bao, Rongming Wang, Qing Zhang, and Yanfeng Zhang**

As an important member of the IVA–VIA group compounds, 2D $SnSe_2$ has emerged as a perfect platform for developing diverse applications, especially in high-performance optoelectronic devices and data storage, etc. However, the bottom-up synthesis of large-area uniform, atomically thin $SnSe_2$ crystals with controlled thicknesses has not yet been realized. Herein, we report the large-area uniform growth of monolayer (1L), bilayer (2L), and few-layer (FL) 1T-$SnSe_2$ single-crystal flakes on mica substrates via a facile chemical vapor deposition (CVD) route. The feeding amount of Sn precursor and flow rate of hydrogen carrier are found to be the key parameters for the thickness-controlled growth of uniform $SnSe_2$ flakes. More intriguingly, obvious second harmonic generation (SHG) is revealed in the retained inversion symmetry structure of 1T-$SnSe_2$, with its intensity showing linear dependence with the thickness from monolayer to multilayers. The new findings reported herein should pave the ways for the thickness-tunable growth of atomically thin $SnSe_2$ crystals, and their unique optical property explorations and applications in nonlinear optics.

J. Fu, L. Zhao, J. Du, X. Wang, J. Song, L. Zhu, F. Zhou, Y. Huan, Q. Zhang, Y. Zhang
School of Materials Science and Engineering
Peking University
Beijing 100871, P. R. China
E-mail: yanfengzhang@pku.edu.cn

L. Zhou, R. Wang
Beijing Advanced Innovation Center for Materials Genome Engineering
Beijing Key Laboratory for Magneto-Photoelectrical Composite and Interface Science
School of Mathematics and Physics
University of Science and Technology
Beijing 100083, P. R. China

K. Wu, L. Bao
Institute of Physics & University of Chinese Academy of Sciences
Chinese Academy of Sciences
Beijing 100190, P. R. China

L. Bao
Songshan Lake Materials Laboratory
Dongguan, Guangdong 523808, P. R. China

The ORCID identification number(s) for the author(s) of this article can be found under https://doi.org/10.1002/admi.202102376.

DOI: 10.1002/admi.202102376

1. Introduction

2D layered materials, including graphene,[1] hexagonal boron nitride (*h*-BN),[2] transition-metal dichalcogenides (TMDCs),[3] IVA–VIA group compounds,[4] etc., have received intensive attention due to their novel physical and chemical properties,[5] and the great application potentials in new-generation electronic and optoelectronic devices.[6–8] As for the diverse IVA–VIA group compounds family, $SnSe_2$ has emerged as a promising n-type semiconducting material for its suitable bandgap (≈1–1.7 eV), good air stability, abundant earth reserve, and environmental-friend advantages.[9,10] Moreover, $SnSe_2$ has served as a perfect platform for exploring some fundamental physical issues, such as pressure-induced metallization,[11] superconductivity,[12] etc., and for developing some novel applications in electrocatalysis,[13,14] thermoelectric,[15,16] data storage,[17,18] high-performance electronic and optoelectronic devices,[10,19] etc.

Particularly, when applied in the optoelectronic field, $SnSe_2$ exhibits high responsivity, ultrafast response rate,[10,19] and satisfactory carrier mobility.[19,20] However, according to previous reports, few-layer (FL) $SnSe_2$-based field effect transistors (FETs) cannot be completely turned off, possibly due to the high electron density ≈10^{18} cm^{-3} in bulk $SnSe_2$,[21] which is significantly higher than that of MoS_2 (≈10^{16} cm^{-3})[22] and black phosphorus (≈10^{15} cm^{-3}).[21] In this regard, FL $SnSe_2$-based electronic devices usually present poor switching ratios, unless a complex top capping layer of polymer electrolyte and HfO_2 (≈70 nm) were selected as the back gate.[21]

In view of this, reducing the thickness of $SnSe_2$ from bulk to FL or even to monolayer (1L), is effective to decrease its electron density, and thus increasing the switching ratio and the related optoelectronic properties. For example, recent experimental results have revealed that, mechanically exfoliated bilayer (2L-) $SnSe_2$ FETs exhibited an on/off ratio of ≈10^3 at room temperature, along with the rise time of ≈2.1 ms and fall time of ≈3.2 ms.[19] Through dielectric engineering or thickness thinning of $SnSe_2$ to atomically thin range may further improve the carrier mobility and boost the response time.

 © 2022 Wiley-VCH GmbH

Notably, most of the existing researches regarding 2D 1T-$SnSe_2$ samples were mainly achieved by the mechanical exfoliation route,[19,21] which customarily induced uncontrollable domain sizes and layer thicknesses, and was incompatible with scalable production. Alternatively, chemical vapor deposition (CVD) presents high efficiency and excellent controllability in the preparation of monolayer 2D materials (e.g., MoS_2,[23] $MoSe_2$,[24] VS_2,[25] etc.). As mentioned above, the photoelectric property of FL or 1L-$SnSe_2$ should be a very intriguing issue. This highly depends on the thickness-tunable growth of 2D 1T-$SnSe_2$ flakes or films with relatively high crystal quality.

In addition, nonlinear optical effects have attracted wide attention in 2D layered materials in the past few years.[26] Existing researches attribute the second harmonic generation (SHG) to the broken inversion symmetry in 2D layered materials, such as 2H-MoS_2[27] and 2H-WS_2[28] monolayers. Novel structures (e.g., 3R-MoS_2,[29,30] folded 1L-MoS_2,[31] spiral WS_2[32]) possessing retained broken inversion symmetry were deliberately created to obtain stronger SHG intensities than their monolayer counterparts. Intriguingly, recent research indicated that mechanically exfoliated multilayer $SnSe_2$ with centrosymmetric lattice arrangement can present second and third harmonic generation (THG) signals.[33,34] However, the internal mechanism of SHG in 1T-$SnSe_2$ is still unclear. Especially, the changing rule of its intensity with layer thickness is still ambiguous, due to the difficulty in achieving strictly layer-controlled growth or exfoliation of atomically thin 1T-$SnSe_2$.

In this work, we have designed an ambient-pressure chemical vapor deposition (APCVD) route to controllably synthesize uniform 1L-, 2L-, and FL-$SnSe_2$ single-crystal flakes on mica substrates. Complementary characterizations by atomic force microscope (AFM), Raman, SHG mapping and high-resolution transmission electron microscopy (HR-TEM) were performed to determine the high crystal quality, 1T-phase lattice structure, and thickness-dependent optical properties of the CVD-derived $SnSe_2$ crystals. We also investigated the nonlinear optical property of the as-grown 1T-$SnSe_2$ flakes on mica as a function of layer thickness, and compared it with mechanically exfoliated 1T-$SnSe_2$ samples on SiO_2/Si. The explicit relationship between SHG response, excitation wavelength, and thicknesses of 1T-$SnSe_2$ was demonstrated. The achieved large-area uniform, thickness-tunable 1T-$SnSe_2$ flakes are expected to serve as perfect platforms for exploring some fundamental physical properties and for developing more broad range applications.

2. Results and Discussion

A facile APCVD route was designed for directly synthesizing atomically thin 1T-$SnSe_2$ with SnI_2 and Se as precursors, as schematically shown in **Figure 1**a. Fluorophlogopite mica ($KMg_3AlSi_3O_{10}F_2$) was selected as the growth substrate in view of its atomic flatness, low surface diffusion barrier and surface inertness, making it a good van der Waals (vdW) epitaxy substrate for growing 2D layer materials.[35,36] Notably, in the published references for the synthesis of 2D 1T-$SnSe_2$, the Se, SnI_2 precursors and mica substrates were placed in sequence in the APCVD chamber (under ≈5 sccm H_2 and ≈20 sccm Ar), leading to the formation of 2L and thicker flakes in the same sample.[10,37]

In this work, to achieve the large-area uniform synthesis of 1L-, 2L-, and FL-$SnSe_2$ flakes, the locations of SnI_2 and Se precursors were deliberately reversed in the CVD system, i.e., the SnI_2 and Se precursors were put at upstream and downstream, respectively. This unique design is selected for significantly lowering the volatilization of the SnI_2 precursor, and thus to realize the uniform synthesis of 1T-$SnSe_2$ flakes with controlled thicknesses. As reported previously, reducing the mass flux of metal precursor was effective to realize the controllable synthesis of uniform 1L and FL 2D layered materials via the CVD method. Specially, thickness-tunable MoS_2[38] and WSe_2[39] were achieved by varying the amount of the NaCl promoter and thus the mass flux of metal precursor. 1L-, 2L-, and FL-$MoSe_2$ were also achieved by increasing the weight of the MoO_3 precursor.[40]

The chemical composition of CVD-grown samples was firstly determined by X-ray photoemission spectroscopy (XPS) on the transferred samples on SiO_2/Si (grown under ≈2 sccm H_2 for ≈15 min) (Figure 1b). Sn $3d_{5/2}$ and $3d_{3/2}$ peaks present at binding energies of ≈486.17 and ≈494.58 eV, while Se $3d_{5/2}$ and $3d_{3/2}$ peaks appear at ≈53.70 and ≈54.56 eV, respectively, in accord with the XPS spectra of molecular beam epitaxy (MBE)-derived $SnSe_2$ thin films on the AlN/Si(111) substrate.[41] Moreover, the X-ray diffraction (XRD) pattern of the transferred $SnSe_2/SiO_2$ was readily indexed to hexagonal $SnSe_2$ (JCPDS 89–2939) with a space group of $P\bar{3}m1$, highly suggesting its 1T-phase crystal structure (Figure 1c). The sharp diffraction peak at ≈14.41° corresponds to the (001) lattice plane of $SnSe_2$.

As shown in the optical microscopy (OM) images in Figure 1d–f, when the H_2 flow rate is set to ≈1.2 sccm, the average domain size of the achieved $SnSe_2$ domains can be tuned from ≈6 to ≈45 µm through increasing the growth time from ≈5 to ≈15 min. Notably, these $SnSe_2$ domains present excellent thickness uniformity (Figure 1d–f), as confirmed tentatively by their uniform OM contrasts. Further representative AFM measurements reveal that, the triangular domain edges present an average thickness of ≈1.4–1.5 nm based on the section-view analyses, highly indicating the uniform 2L feature (Figure 1g and Figure S1, Supporting Information, grown under ≈1.2 sccm H_2 for ≈10 min).

However, when the sample was synthesized under ≈0.4 sccm H_2 for ≈15 min, $SnSe_2$ was hardly observed in the OM image (Figure S2a, Supporting Information). It is thus proposed that, the growth of $SnSe_2$ requires the participation and promotion of H_2. The possible reaction route is as follows,

$$SnI_2 + 2Se + H_2 = SnSe_2 + 2HI \quad (1)$$

According to previous reports, when H_2 participates in the chemical reaction in the CVD process, the concentration of H_2 carrier can effectively adjust the layer thickness of 2D nanoflakes. For example, 1L-WSe_2[39] and ultrathin VS_2 (4–8 nm)[42] samples were obtained by reducing the H_2 flow rate. Especially, Chen et al. reported the thickness-controlled growth of 1L-, 2L- and multilayer $MoSe_2$ flakes by varying the H_2 flow rate from 3, 5 to 6 sccm, respectively.[40]

In contrast, for the sample grown under ≈0.8 sccm H_2 for ≈15 min, the $SnSe_2$ flakes present a uniform and lighter

© 2022 Wiley-VCH GmbH

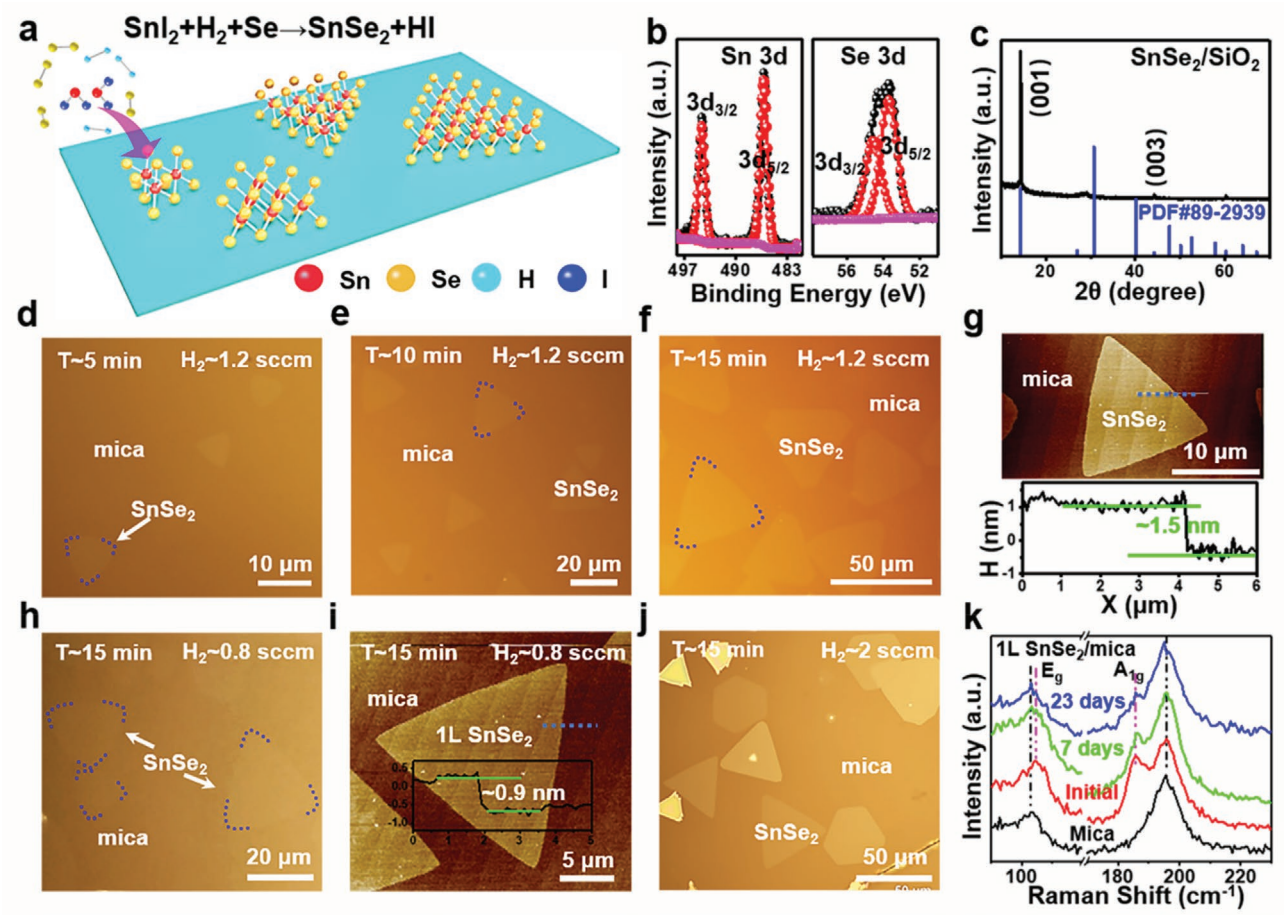

Figure 1. Thickness-tunable growth of atomically thin 1T-$SnSe_2$ flakes on mica by an APCVD route. a) Schematic of the APCVD growth process. b) XPS spectra regarding Sn and Se elements for FL-$SnSe_2$ transferred on SiO_2/Si. c) XRD pattern of transferred FL-$SnSe_2$ on SiO_2/Si, showing its 1T-phase feature. d–f) OM images of as-grown $SnSe_2$ flakes on mica, showing gradually increased domain sizes (from ≈6 to ≈45 µm) by increasing growth time from ≈5 to ≈15 min under ≈1.2 sccm H_2 and ≈20 sccm Ar. g) Representative AFM image and corresponding height profile of the 2L-$SnSe_2$ flake (≈1.5 nm) synthesized on mica as shown in (e). h, i) OM image, AFM image and corresponding height profile of the 1L-$SnSe_2$ flakes (≈0.9 nm) synthesized on mica under ≈0.8 sccm H_2 and ≈20 sccm Ar for ≈15 min. j) OM image of the as-grown $SnSe_2$ flakes synthesized under ≈2 sccm H_2 and ≈20 sccm Ar for ≈15 min, showing varied thicknesses from 2L to FL. k) Raman spectra of mica, and freshly synthesized, 7 and 23 days aged 1L-$SnSe_2$ flakes on mica (in air), presenting invariable peak position and thus robust stability in air.

contrasts than those grown under ≈1.2 sccm H_2, along with decreased domain sizes ≈20 µm (Figure 1h). Based on the AFM image in Figure 1i, the obtained $SnSe_2$ flakes own an average height of ≈0.9 nm, in good agreement with the monolayer thickness. Similarly, decreasing the growth time from ≈15 to ≈10 min results in a gradual decrease of the domain size from ≈20 µm to ≈8 µm (Figure S2b, Supporting Information). The excellent thickness uniformity of the samples was further confirmed by the uniform contrast in the OM image (Figure S2c, Supporting Information). Briefly, homogeneous 1L-$SnSe_2$ flakes are successfully synthesized on the mica substrate under the current synthetic design. This is the first CVD growth of uniform 1L 1T-$SnSe_2$ flakes with relatively large domain sizes.

When the H_2 flow rate was increased to ≈2 sccm, the CVD-grown $SnSe_2$ flakes show darker and discrepant contrasts (Figure 1j), indicating the formation of trilayer (3L-) and even thicker flakes. This may be due to the feeding of excessive active precursor species, or the formation of larger precursor clusters at an elevated H_2 concentration. Moreover, the average domain sizes of $SnSe_2$ flakes present a gradual decrease to ≈15 µm with decreasing the growth time to ≈10 min (Figure S2d, Supporting Information).

In short, the flow rate of H_2 in the APCVD growth system is critical for the thickness-controlled growth of uniform $SnSe_2$ flakes. A low H_2 concentration leads to the generation of fewer active precursors, and slow surface reaction rate, favorable for the growth of uniform 1L- or 2L-$SnSe_2$ flakes. When the H_2 concentration is dramatically increased, excessive active precursor species can be produced to facilitate the growth along the out-of-plane direction and eventually form thicker $SnSe_2$ flakes. Overall, growth time is also a key factor for enlarging the domain size of the thickness-uniform $SnSe_2$ flakes under the optimized growth condition.

The stability of atomically thin or 1L 1T-$SnSe_2$ is also a very critical issue for further applications. Raman spectra of freshly synthesized, 7 and 23 days aged 1L-$SnSe_2$ flakes on mica were also examined carefully (Figure 1k). No obvious changes in peak position/intensity for 1L 1T-$SnSe_2$ flakes (E_g for in-plane

 © 2022 Wiley-VCH GmbH

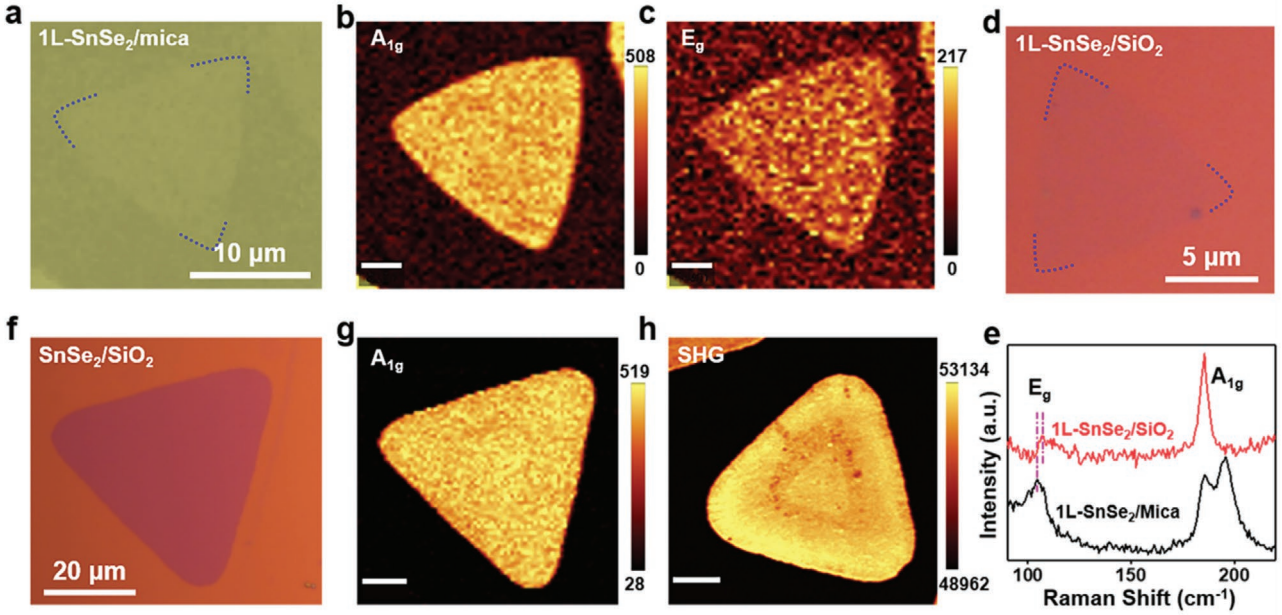

Figure 2. Spectroscopic characterizations of as-grown triangular $SnSe_2$ flakes and after being transferred on SiO_2/Si. a–c) OM image of as-grown triangular 1L-$SnSe_2$ flake on mica (grown under ≈0.8 sccm H_2 for 15 min) and corresponding Raman mapping images on A_{1g} and E_g peak intensities, respectively. Scale bars in (b) and (c): 3 µm. d) OM image of 1L-$SnSe_2$ flake transferred on SiO_2/Si. e) Raman spectra of 1L-$SnSe_2$ as-grown on mica and transferred on SiO_2/Si. f, g) Representative OM image of FL-$SnSe_2$ (≈3–4L, grown under ≈2 sccm H_2 for 15 min) transferred on SiO_2/Si and corresponding Raman mapping regarding A_{1g} peak intensity. h) SHG mapping of FL-$SnSe_2$ (≈4-5L) transferred on SiO_2/Si. Scale bars in (g) and (h): 10 µm.

vibration mode of Se atoms ≈104.8 cm^{-1}, and A_{1g} for out-of-plane vibration mode ≈185.7 cm^{-1}) occur even after 23 days reservation in air, indicating the robust stability of CVD-derived sample.[10,19] The mica substrate has two significant peaks at ≈103.3 and ≈195.0 cm^{-1}. In this regard, air-stable, domain size and thickness-tunable 1T-$SnSe_2$ have been successfully synthesized on mica substrates by a facile APCVD route.

Raman mapping was also performed on the as-grown 1L-$SnSe_2$ flake on mica, with its OM image shown in **Figure 2**a. The Raman mapping images regarding A_{1g} and E_g peak intensity (Figure 2b, c, respectively) present homogeneous contrast in the $SnSe_2$ areas, again indicating the uniform monolayer feature. For comparison, Raman measurement was also carried out on the transferred 1L-$SnSe_2$ flake. Note that, the OM image of the transferred 1L-$SnSe_2$ flake exhibits extremely dim contrast, due to its extremely thin thickness (Figure 2d). The E_g Raman mode (Figure 2e) shows an obvious blueshift from ≈104.8 to ≈106.7 cm^{-1} before and after the transfer process. This is expected to be due to the compressive strain effect induced by adlayer-substrate lattice mismatch (a_{SnSe2} = 0.381 nm, $\sqrt{3}a_{SnSe2}$ = 0.660 nm and a_{mica} = 0.531 nm). Similar blueshifts were also reported for $ReSe_2$/Au and $PtSe_2$/Au foil, and attributed to compressive strain effect and strong interfacial interaction between adlayers and Au substrates.[43,44]

Raman mapping was also performed on the transferred FL-$SnSe_2$ on SiO_2/Si substrates. The homogeneous OM contrast image and Raman mapping images regarding the A_{1g} peak intensity, full width at half maximum (FWHM) of A_{1g} peak and E_g peak intensity (Figure 2f,g, S3a,b, Supporting Information, respectively), collectively indicate the uniform thickness feature of the CVD-grown $SnSe_2$. Moreover, no distinct internal grain structure is observed on the transferred FL-$SnSe_2$ on SiO_2/Si, according to the SHG mapping image (Figure 2h, OM image in Figure S3c, Supporting Information). The triangular flakes synthesized in our work should be single-crystal domains, similar to the photoluminescence (PL) mapping results for single-crystal 1L-WSe_2 and WS_2 samples.[45] The darker spots on them are probably derived from the harsh sample transfer process.

HR-TEM characterization was then performed to examine the crystal quality of the CVD-derived $SnSe_2$ samples. **Figure 3**a shows a low-magnification TEM image of a typical triangular $SnSe_2$ flake with an edge length of ≈23 µm. Some wrinkles and breakages observed herein are attributed to the harsh transfer process. The selected-area electron diffraction (SAED) patterns (Figure 3b–d) collected from the three numbered regions (1, 2, and 3 in Figure 3a) present hexagonal diffraction spots, suggesting the hexagonal crystal structure of the derived $SnSe_2$ sample. Moreover, nearly perfect coincidence (deviation smaller than ±0.5°) among the different SAED patterns again indicates the single-crystal nature of the triangular $SnSe_2$ flake.

Moreover, the typical HR-TEM image of the $SnSe_2$ flake (Figure 3e) presents a perfect atomic structure with the lattice spacing of ≈0.33 nm, in good coincidence with the published data for mechanically exfoliated or CVD-synthesized 1T-$SnSe_2$ flakes.[10,19] Moreover, the corresponding fast Fourier transform (FFT) pattern (inset of Figure 3e) presents sixfold-symmetric spots, again indicating the hexagonal lattice structure of the $SnSe_2$ sample. Additional energy dispersive X-ray spectroscopy (EDX) elemental mapping images (Figure 3f,g) reveal uniform spatial distribution of Sn and Se elements (around the highlighted rectangle area in Figure 3a), along with an element ratio of Sn/Se ≈1:2.07 (Figure 3h). In this regard, the CVD-derived

© 2022 Wiley-VCH GmbH

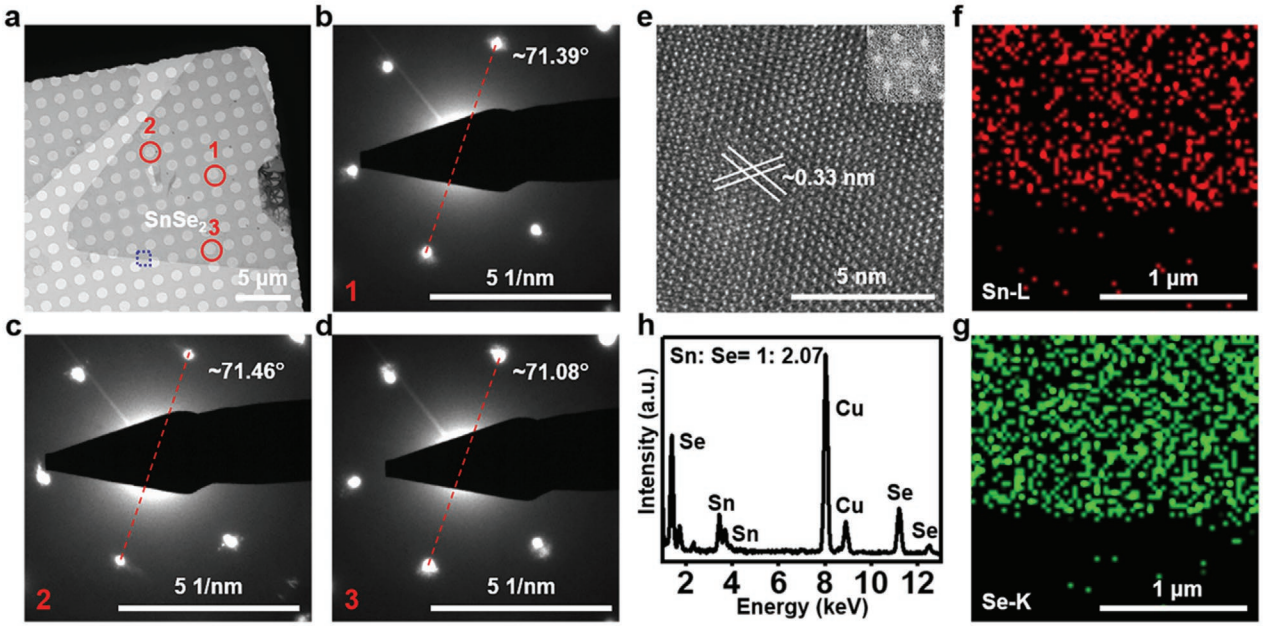

Figure 3. Representative TEM characterizations of a few-layer triangular 1T-$SnSe_2$ flake. a) Low-magnification TEM image of a few-layer $SnSe_2$ flake transferred on a Cu TEM grid. b-d) SAED patterns from the regions highlighted by red circles numbered by 1–3 in (a). The rotation angles of the three red dotted lines with respect to the horizontal line are ≈71.39°, 71.46° and 71.08°, respectively, indicating the single-crystal nature of the triangular flake. e) Corresponding HR-TEM image of the $SnSe_2$ flake in (a), showing a lattice constant of ≈0.33 nm. Inset: corresponding FFT pattern. f, g) Sn and Se elements mapping images of the highlighted rectangle area in (a) (around the flake edge location). h) Corresponding EDX spectrum of the selected area in (f) and (g).

triangular $SnSe_2$ flakes are single-crystal domains with a 1T-phase structure and relatively high crystal quality.

Due to centrosymmetric lattice arrangement of atomically 1T-$SnSe_2$, it is normally expected to exhibit a vanishing nonlinear optical effect. However, spatially-resolved SHG and THG have been recently reported from multilayer 1T-$SnSe_2$ flakes, using a nonlinear optical microscopy setup.[33] In this work, the atomically thin 1T-$SnSe_2$ flakes with well-defined thicknesses allow establishing a more direct correlation between layer thickness and the nonlinear optical property. Raman and SHG spectra of 1–8L 1T-$SnSe_2$ single-crystal flakes were thus achieved directly on mica substrates and after being transferred on SiO_2/Si substrates. A direct comparison of the two types of samples with the mechanically exfoliated ones from bulk 1T-$SnSe_2$ crystals was also performed to achieve a clearer understanding of the thickness-dependent optical properties.

Firstly, 1–8L triangular shaped $SnSe_2$ flakes with neat edges were selected as candidates, with the layer thicknesses determined definitely by AFM height profile measurements (Figure S4, Supporting Information). Corresponding Raman spectra were collected in **Figure 4**a. The Raman E_g and A_{1g} peak position variations with layer thicknesses are displayed in Figure 4c and Table S1, Supporting Information. Evidently, the intensity of the Raman signal increases significantly with increasing the layer thickness from 1L to 8L (Figure S5, Supporting Information), due to the increase of scattering centers in thicker $SnSe_2$ flakes as reported previously.[10]

Specifically, the E_g mode for CVD-grown $SnSe_2$ on mica shows an obvious blueshift (from ≈104.8, 107.1, 112.2 to 115.3 cm^{-1}), with the thickness varying from 1L, 2L, 3L to 4L, different from common TMDCs materials showing a normal redshift (e.g., MoS_2,[46] $PtSe_2$[44] and ReS_2[47]). The significant blueshift for the in-plane vibration mode (E_g) with increasing the layer thickness, may be attributed to the increased in-plane coupling. This obvious in-plane vibration mode blueshift with increasing the layer thickness was also reported in the metal monochalcogenides (MX) from IVA–VIA group.[48] Moreover, the E_g and A_{1g} peak positions of 5–8L as-grown samples are basically consistent with those of the mechanically exfoliated 5–8L flakes from bulk crystals on SiO_2/Si (shown in Figure 4c and S8, Supporting Information), and the exfoliated $SnSe_2$ samples reported previously.[49] That means thicker flakes (above 4L) present normal vibration states, regardless the thickness effect and the strain effect from the substrates.

For the transferred CVD-grown 1T-$SnSe_2$ flakes on SiO_2 substrates (Figure S6, Supporting Information), the E_g peak positions (Figure 4b,c) present an obvious blueshift (≈9.4 cm^{-1}) by increasing the layer number from 1L to 4L and stabilizes at >4L. The A_{1g} peak position shows only a minor fluctuation from 1L to 8L (Table S1, Supporting Information), basically consistent with that of the mechanically exfoliated 1T-$SnSe_2$ layers from bulk crystals achieved in this work. However, the A_{1g} peak intensity increases significantly from 1L to 8L (Figure S5, Supporting Information). In this regard, the as-grown 1T-$SnSe_2$ layers on the mica substrate are expected to be a little strained, as inferred by the minor change of E_g peak position with regard to the transferred or mechanically exfoliated layers. Briefly, this definitely defined thickness-dependent Raman A_{1g} peak intensity and E_g peak positions can be used as a good criterion to identify the thickness of few-layer samples.

 © 2022 Wiley-VCH GmbH

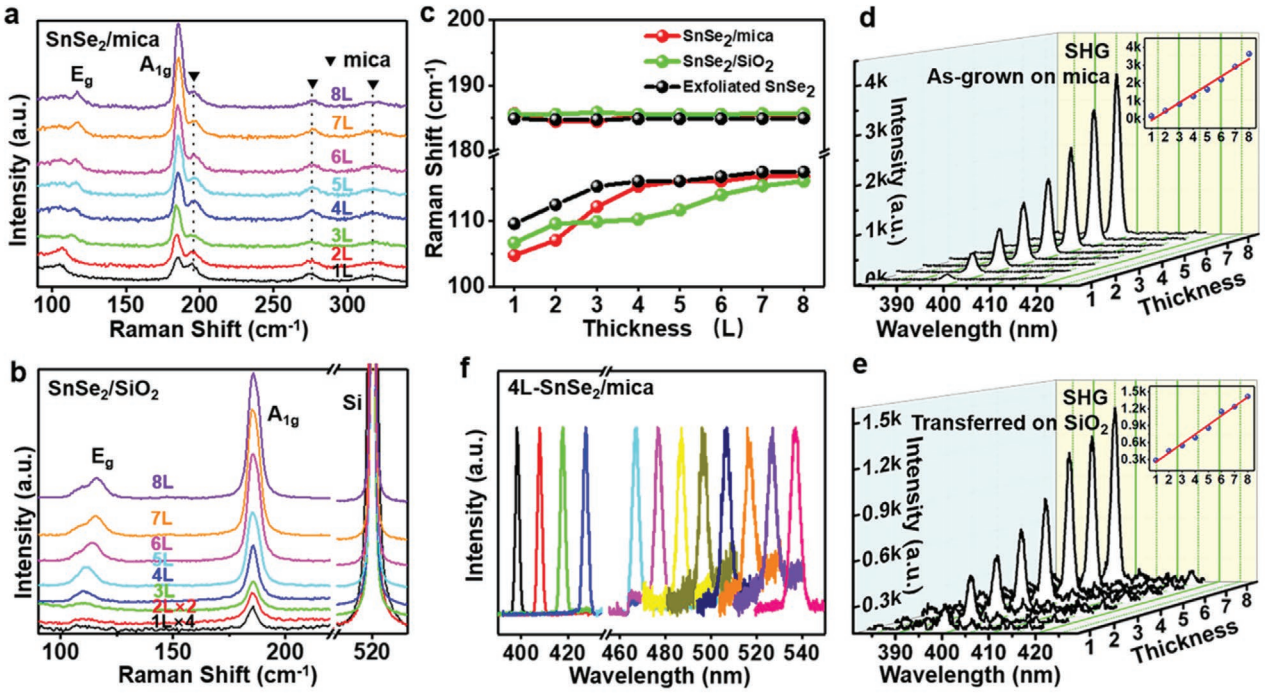

Figure 4. Thickness and wavelength dependence of Raman spectrum and SHG intensity of as-grown triangular 1T-$SnSe_2$ flakes on mica and transferred on SiO_2/Si as a function of layer thickness. a) Raman spectra of 1–8L 1T-$SnSe_2$ flakes captured from the as-grown samples on mica. The excitation wavelength is 532 nm. b) Thickness-dependent Raman spectra of 1–8L 1T-$SnSe_2$ flakes after being transferred on SiO_2/Si. c) Evolution of the E_g and A_{1g} peak positions with increasing the thicknesses of as-grown 1T-$SnSe_2$ on mica and transferred on SiO_2/Si (marked with red and green balls), with the mechanically exfoliated ones from bulk 1T-$SnSe_2$ crystals as a reference (with black balls). d, e) Thickness-dependent SHG spectra of 1–8L 1T-$SnSe_2$ flakes as-grown on mica and transferred on SiO_2/Si under a fixed excitation wavelength ≈800 nm. Inset plots show a similar linear correlation between SHG peak intensity and layer thickness. f) Wavelength-dependent SHG spectra under varied excitation wavelength (from 800 to 1080 nm).

Subsequently, SHG spectra of 1–8L 1T-$SnSe_2$ were also achieved directly on mica and after being transferred on SiO_2/Si substrates. The SHG signal intensity (Figure 4d,e) can be noticed to show a linear increase from 1L to 8L. Moreover, a broad available band can be achieved for the generation of SHG signal, as evidenced by the test on a 4L-$SnSe_2$ flake with the excitation wavelength ranging from 800 to 1080 nm (Figure 4e).

In order to determine the origin of the SHG signal in $SnSe_2$, and to eliminate the influences of lattice defects and stress. Mechanical exfoliation of a coexisted FL 1T-$SnSe_2$ sample was also performed on SiO_2/Si with an Au/Ti adhesion layer, via a universal Au-assisted exfoliation method from a bulk single crystal.[50] As shown by the OM image in **Figure 5**a, the obtained $SnSe_2$ sample show discrepant contrasts with lateral sizes of ≈5 µm for the different thickness regions.

Their thicknesses (1-8L) were definitely defined by the AFM height profile analysis (Figure 5b,c and Figure S7, Supporting Information). Considering the monolayer thickness of ≈0.62 nm,[10,19] and the measurement error of AFM analysis, the average height of ≈0.6–0.7 nm was attributed to that of 1L-$SnSe_2$, and the average height of ≈1.8–1.9 nm was assigned to that of 3L-$SnSe_2$.

Eight typical SHG spectra (Figure 5d) and Raman spectra (Figure S8, Supporting Information) were collected from the 1–8L $SnSe_2$ regions. No obvious damage due to the laser irradiation was observed according to the OM image of the mechanically exfoliated 1T-$SnSe_2$ sample after Raman and SHG characterizations (Figure S7c, Supporting Information). The intensity of SHG shows a linear increase with increasing the layer thickness of $SnSe_2$, indicating that the SHG signal arises from $SnSe_2$ itself. Herein, the SHG intensity of the few-layer sample should be the accumulation of each composite layer. A similar result was also reported in spiral WS_2 structures, possessing linearly increased SHG intensity, other than diminishing the oscillation of 2H stacking TMDs.[32] However, the SHG intensity of monolayer 1T-$SnSe_2$ is much lower than that of monolayer 2H-WS_2 and MoS_2 (Figure S9, Supporting Information), and only stronger than that of 2L 2H-WS_2 with restored inversion symmetry (Figure 5e). This disparity may be attributed to the different lattice structures (1T versus 2H), or the different SHG mechanisms. In the reported references, the SHG signals of mechanically exfoliated multilayer $SnSe_2$ with centrosymmetric lattice arrangement were loosely correlated to crystal lattice distortion.[33,34] The CVD-derived 1T-$SnSe_2$ flakes should have the similar property with the mechanically exfoliated ones, as confirmed by comparative spectroscopy data, and the SHG should follow the similar mechanism.

3. Conclusion

In summary, we have accomplished the controllable synthesis of large-area uniform 1L, 2L, and FL 1T-$SnSe_2$ flakes on mica substrates by designing a unique synthetic route. The achieved

© 2022 Wiley-VCH GmbH

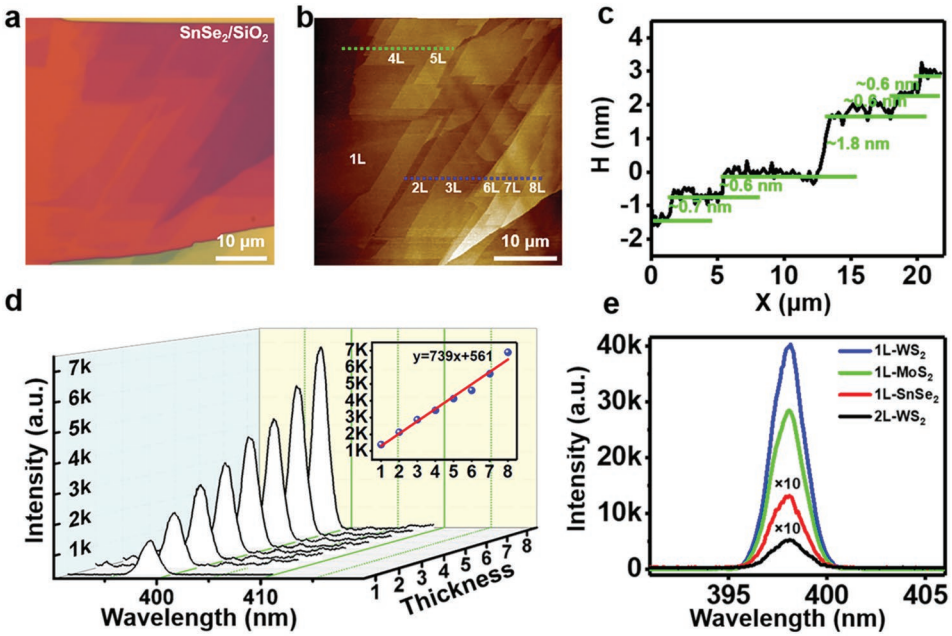

Figure 5. Thickness-dependent SHG intensity of a mechanically exfoliated 1T-$SnSe_2$ sample on SiO_2/Si with a Au/Ti adhesion layer via a universal Au-assisted exfoliation method. a, b) OM image and corresponding AFM image of the mechanically exfoliated 1T-$SnSe_2$ sample on SiO_2/Si, showing the thickness variation from 1–8L. c) Corresponding height profile collected from the blue dotted line in b), confirming the thickness distribution. d) Thickness-dependent SHG spectra of the 1T-$SnSe_2$ sample, under a fixed excitation wavelength at 800 nm. Inset image shows a linear relation between SHG peak intensity and the layer number. e) Comparison of SHG spectra for the mechanically exfoliated 1L-WS_2, 1L-MoS_2, 1L-$SnSe_2$, and 2L-WS_2 samples on SiO_2.

high-quality single-crystal $SnSe_2$ flakes with well-defined thicknesses (1–8L) provide perfect platforms for exploring the thickness-dependent Raman and SHG properties for the first time. SHG signals were detected in the centrosymmetric lattice structure of 1T-$SnSe_2$ on both mica and SiO_2/Si substrates, presenting a linear dependence with the layer thickness. This unconventional phenomenon of SHG will inspire new interests in exploring the basic nonlinear optical properties of 2D layer materials with an inversion symmetry structure. This work should hereby pave the ways for the thickness-controlled growth of atomically thin 1T-$SnSe_2$ crystals, and promote fundamental property explorations and practical applications in more versatile fields.

4. Experimental Section

Synthesis of Atomically Thin 1T-$SnSe_2$ Flakes and the Sample Transfer Process: The growth of $SnSe_2$ was completed in a single-temperature-zone CVD furnace (Lindberg/Blue M) equipped with a 1 in.-diameter quartz tube. SnI_2 pellets (Alfa Aesar; purity 99.999%; 20 mg) were placed at ≈15.5 cm away from the center of the furnace. The Se powder (Alfa Aesar; purity 99.5%; 0.1 g) was placed next to it on the right. Freshly cleaved fluorophlogopite mica substrates were put at ≈15.5 cm downstream from the center of the furnace over a quartz boat. The typical growth temperature was set to ≈600 °C and kept at the set point for 5–15 min under atmospheric pressure. Ar (20 sccm) and H_2 (0.8–2 sccm) were used as carrier gases during the APCVD growth process. The as-grown samples were transferred on arbitrary substrates by using polystyrene (PS) as a supporting polymer, as reported for CVD-derived hexagonal phase $FeTe_2$ (*h*-$FeTe_2$) nanoflakes grown on mica.[51]

Material Characterizations: The CVD-derived $SnSe_2$ flakes as-grown on mica and transferred on SiO_2/Si were systematically characterized by OM (Olympus BX51), XPS (Kratos Analytical AXIS-Ultra fitted with a monochromatic Al Kα X-ray source), SEM (Hitachi S-4800, 3 kV), XRD (Shimadzu Thin Film, using Cu Kα radiation in the 2θ range of 10 ≈ 90°), Raman (Renishaw, Invia Reflex), TEM (JEOL JEM-2100F LaB6; acceleration voltage, 200 kV), AFM (Dimension Icon, Bruker) and SHG spectroscopy (Alpha 300R, WITec).

Supporting Information

Supporting Information is available from the Wiley Online Library or from the author.

Acknowledgements

This work was financially supported by the National Key Research and Development Program of China (No. 2018YFA0703700), the National Natural Science Foundation of China (Nos. 51925201, 51991340, 51991344, 51971025, and 12034002), Natural Science Foundation of Beijing, China (No. 2212034), the Open Research Fund Program of the State Key Laboratory of Low Dimensional Quantum Physics (No. KF202011), the China Postdoctoral Science Foundation (No. 2021M690195), and Chinese Academy of Sciences (XDB30000000, Y201902).

Conflict of Interest

The authors declare no conflict of interest.

Data Availability Statement

Research data are not shared.

 © 2022 Wiley-VCH GmbH

Keywords

chemical vapor deposition, monolayer, second harmonic generation (SHG), $SnSe_2$, uniform growth of $SnSe_2$ flakes

Received: December 3, 2021
Revised: February 5, 2022
Published online:

[1] K. S. Novoselov, A. K. Geim, S. V. Morozov, D. Jiang, M. I. Katsnelson, I. V. Grigorieva, S. V. Dubonos, A. A. Firsov, *Nature* **2005**, *438*, 197.
[2] S. M. Kim, A. Hsu, M. H. Park, S. H. Chae, S. J. Yun, J. S. Lee, D.-H. Cho, W. Fang, C. Lee, T. Palacios, M. Dresselhaus, K. K. Kim, Y. H. Lee, J. Kong, *Nat. Commun.* **2015**, *6*, 8662.
[3] W. Chen, J. Zhao, J. Zhang, L. Gu, Z. Yang, X. Li, H. Yu, X. Zhu, R. Yang, D. Shi, X. Lin, J. Guo, X. Bai, G. Zhang, *J. Am. Chem. Soc.* **2015**, *137*, 15632.
[4] G. Su, V. G. Hadjiev, P. E. Loya, J. Zhang, S. Lei, S. Maharjan, P. Dong, P. M. Ajayan, J. Lou, H. Peng, *Nano Lett.* **2015**, *15*, 506.
[5] K. F. Mak, C. Lee, J. Hone, J. Shan, T. F. Heinz, *Phys. Rev. Lett.* **2010**, *105*, 136805.
[6] Q. Fu, L. Yang, W. Wang, A. Han, J. Huang, P. Du, Z. Fan, J. Zhang, B. Xiang, *Adv. Mater.* **2015**, *27*, 4732.
[7] Y. Huang, H. X. Deng, K. Xu, Z. X. Wang, Q. S. Wang, F. M. Wang, F. Wang, X. Y. Zhan, S. S. Li, J. W. Luo, J. He, *Nanoscale* **2015**, *7*, 14093.
[8] Y. Huang, K. Xu, Z. Wang, T. A. Shifa, Q. Wang, F. Wang, C. Jiang, J. He, *Nanoscale* **2015**, *7*, 17375.
[9] J. M. Gonzalez, I. I. Oleynik, *Phys. Rev. B* **2016**, *94*, 125443.
[10] X. Zhou, L. Gan, W. Tian, Q. Zhang, S. Jin, H. Li, Y. Bando, D. Golberg, T. Zhai, *Adv. Mater.* **2015**, *27*, 8035.
[11] Y. Zhou, B. Zhang, X. Chen, C. Gu, C. An, Y. Zhou, K. Cai, Y. Yuan, C. Chen, H. Wu, R. Zhang, C. Park, Y. Xiong, X. Zhang, K. Wang, Z. Yang, *Adv. Electron. Mater.* **2018**, *4*, 1800155.
[12] Y.-M. Zhang, J.-Q. Fan, W.-L. Wang, D. Zhang, L. Wang, W. Li, K. He, C.-L. Song, X.-C. Ma, Q.-K. Xue, *Phys. Rev. B* **2018**, *98*, 220508.
[13] B. He, L. Jia, Y. Cui, W. Zhou, J. Sun, J. Xu, Q. Wang, L. Zhao, *ACS Appl. Energy Mater.* **2019**, *2*, 7655.
[14] Y. Liu, Y. Xu, Y. Han, Z. Zhang, J. Xu, Y. Du, J. Bao, X. Zhou, *J. Power Sources* **2019**, *436*, 226860.
[15] Y. Luo, Y. Zheng, Z. Luo, S. Hao, C. Du, Q. Liang, Z. Li, K. A. Khor, K. Hippalgaonkar, J. Xu, Q. Yan, C. Wolverton, M. G. Kanatzidis, *Adv. Energy Mater.* **2018**, *8*, 1702167.
[16] C. Zhou, Y. Yu, X. Zhang, Y. Cheng, J. Xu, Y. K. Lee, B. Yoo, O. Cojocaru-Mirédin, G. Liu, S.-P. Cho, M. Wuttig, T. Hyeon, I. Chung, *Adv. Funct. Mater.* **2020**, *30*, 1908405.
[17] M. Micoulaut, W. Wełnic, M. Wuttig, *Phys. Rev. B* **2008**, *78*, 224209.
[18] K.-M. Chung, D. Wamwangi, M. Woda, M. Wuttig, W. Bensch, *J. Appl. Phys.* **2008**, *103*, 083523.
[19] P. Yu, X. Yu, W. Lu, H. Lin, L. Sun, K. Du, F. Liu, W. Fu, Q. Zeng, Z. Shen, C. Jin, Q. J. Wang, Z. Liu, *Adv. Funct. Mater.* **2016**, *26*, 137.
[20] Y. Su, M. A. Ebrish, E. J. Olson, S. J. Koester, *Appl. Phys. Lett.* **2013**, *103*, 263104.
[21] T. Pei, L. Bao, G. Wang, R. Ma, H. Yang, J. Li, C. Gu, S. Pantelides, S. Du, H.-j. Gao, *Appl. Phys. Lett.* **2016**, *108*, 053506.
[22] D. M. D'Ambra, J. V. Marzik, R. Kershaw, J. Baglio, K. Dwight, A. Wold, *J. Solid State Chem.* **1985**, *57*, 351.
[23] S. Najmaei, Z. Liu, W. Zhou, X. Zou, G. Shi, S. Lei, B. I. Yakobson, J.-C. Idrobo, P. M. Ajayan, J. Lou, *Nat. Mater.* **2013**, *12*, 754.
[24] J. Zhou, J. Lin, X. Huang, Y. Zhou, Y. Chen, J. Xia, H. Wang, Y. Xie, H. Yu, J. Lei, D. Wu, F. Liu, Q. Fu, Q. Zeng, C.-H. Hsu, C. Yang, L. Lu, T. Yu, Z. Shen, H. Lin, B. I. Yakobson, Q. Liu, K. Suenaga, G. Liu, Z. Liu, *Nature* **2018**, *556*, 355.
[25] J. Yuan, J. Wu, W. J. Hardy, P. Loya, M. Lou, Y. Yang, S. Najmaei, M. Jiang, F. Qin, K. Keyshar, H. Ji, W. Gao, J. Bao, J. Kono, D. Natelson, P. M. Ajayan, J. Lou, *Adv. Mater.* **2015**, *27*, 5605.
[26] Z. Sun, A. Martinez, F. Wang, *Nat. Photonics* **2016**, *10*, 227.
[27] X. Yin, Z. Ye, A. Chenet Daniel, Y. Ye, K. O'Brien, C. Hone James, X. Zhang, *Science* **2014**, *344*, 488.
[28] C. Janisch, Y. Wang, D. Ma, N. Mehta, A. L. Elías, N. Perea-López, M. Terrones, V. Crespi, Z. Liu, *Sci. Rep.* **2014**, *4*, 5530.
[29] J. Shi, P. Yu, F. Liu, P. He, R. Wang, L. Qin, J. Zhou, X. Li, J. Zhou, X. Sui, S. Zhang, Y. Zhang, Q. Zhang, T. C. Sum, X. Qiu, Z. Liu, X. Liu, *Adv. Mater.* **2017**, *29*, 1701486.
[30] M. Zhao, Z. Ye, R. Suzuki, Y. Ye, H. Zhu, J. Xiao, Y. Wang, Y. Iwasa, X. Zhang, *Light: Sci. Appl.* **2016**, *5*, e16131.
[31] T. Jiang, H. Liu, D. Huang, S. Zhang, Y. Li, X. Gong, Y.-R. Shen, W.-T. Liu, S. Wu, *Nat. Nanotechnol.* **2014**, *9*, 825.
[32] X. Fan, Y. Jiang, X. Zhuang, H. Liu, T. Xu, W. Zheng, P. Fan, H. Li, X. Wu, X. Zhu, Q. Zhang, H. Zhou, W. Hu, X. Wang, L. Sun, X. Duan, A. Pan, *ACS Nano* **2017**, *11*, 4892.
[33] R. Biswas, M. Dandu, A. Prosad, S. Menon, K. Majumdar, V. Raghunathan, *IEEE Comput. Soc.* **2019**, 30.
[34] B. Rabindra, D. Medha, J. Keshav Kumar, M. Sruti, K. M. Jyothsna, M. Kaushik, R. Varun, *Proc. of SPIE* **2020**, *11282*.
[35] Q. Ji, Y. Zhang, T. Gao, Y. Zhang, D. Ma, M. Liu, Y. Chen, X. Qiao, P.-H. Tan, M. Kan, J. Feng, Q. Sun, Z. Liu, *Nano Lett.* **2013**, *13*, 3870.
[36] L. Huang, Y. Yu, C. Li, L. Cao, *J. Phys. Chem., C* **2013**, *117*, 6469.
[37] B. An, Y. Ma, G. Zhang, C. You, Y. Zhang, *RSC Adv.* **2020**, *10*, 42157.
[38] P. Yang, Z. Zhang, M. Sun, F. Lin, T. Cheng, J. Shi, C. Xie, Y. Shi, S. Jiang, Y. Huan, P. Liu, F. Ding, C. Xiong, D. Xie, Y. Zhang, *ACS Nano* **2019**, *13*, 3649.
[39] Q. Feng, M. Zhu, Y. Zhao, H. Liu, M. Li, J. Zheng, H. Xu, Y. Jiang, *Nanotechnology* **2018**, *30*, 034001.
[40] T. Chen, G. Hao, G. Wang, B. Li, L. Kou, H. Yang, X. Zheng, J. Zhong, *2D Mater.* **2019**, *6*, 025002.
[41] K. E. Aretouli, D. Tsoutsou, P. Tsipas, J. Marquez-Velasco, S. Aminalragia Giamini, N. Kelaidis, V. Psycharis, A. Dimoulas, *ACS Appl. Mater. Interfaces* **2016**, *8*, 23222.
[42] Q. Ji, C. Li, J. Wang, J. Niu, Y. Gong, Z. Zhang, Q. Fang, Y. Zhang, J. Shi, L. Liao, X. Wu, L. Gu, Z. Liu, Y. Zhang, *Nano Lett.* **2017**, *17*, 4908.
[43] C. Xie, S. Jiang, X. Zou, Y. Sun, L. Zhao, M. Hong, S. Chen, Y. Huan, J. Shi, X. Zhou, Z. Zhang, P. Yang, Y. Shi, P. Liu, Q. Zhang, P. Gao, Y. Zhang, *Nano Res.* **2019**, *12*, 149.
[44] J. Fu, M. Hong, J. Shi, C. Xie, S. Jiang, Q. Shang, Q. Zhang, Y. Shi, Y. Huan, Z. Zhang, P. Yang, X. Li, L. Gu, Q. Zhang, C. Shan, Y. Zhang, *ACS Appl. Mater. Interfaces* **2019**, *11*, 48221.
[45] S. Li, S. Wang, D.-M. Tang, W. Zhao, H. Xu, L. Chu, Y. Bando, D. Golberg, G. Eda, *Appl. Mater. Today* **2015**, *1*, 60.
[46] C. Lee, H. Yan, L. E. Brus, T. F. Heinz, J. Hone, S. Ryu, *ACS Nano* **2010**, *4*, 2695.
[47] M. Hafeez, S. ur Rehman, A. S. Saleemi, M. Saeed, L. Zhu, *Appl. Surf. Sci.* **2019**, *493*, 1215.
[48] M. Park, J. S. Choi, L. Yang, H. Lee, *Sci. Rep.* **2019**, *9*, 19826.
[49] D. G. Mead, J. C. Irwin, *Solid State Commun.* **1976**, *20*, 885.
[50] Y. Huang, Y.-H. Pan, R. Yang, L.-H. Bao, L. Meng, H.-L. Luo, Y.-Q. Cai, G.-D. Liu, W.-J. Zhao, Z. Zhou, L.-M. Wu, Z.-L. Zhu, M. Huang, L.-W. Liu, L. Liu, P. Cheng, K.-H. Wu, S.-B. Tian, C.-Z. Gu, Y.-G. Shi, Y.-F. Guo, Z. G. Cheng, J.-P. Hu, L. Zhao, G.-H. Yang, E. Sutter, P. Sutter, Y.-L. Wang, W. Ji, X.-J. Zhou, et al., *Nat. Commun.* **2020**, *11*, 2453.
[51] S. Chen, H. Liu, F. Chen, K. Zhou, Y. Xue, *ACS Nano* **2020**, *14*, 11473.

 © 2022 Wiley-VCH GmbH